Volume 16, Number 4, 2023. pp. 435-445

Jordan Journal of Physics

ARTICLE

Magnetization Plateaus of a Double Fullerene Core/Shell Like-Nanostructure in an External Magnetic Field: Monte Carlo Study

H. Eraki, N. Maaouni, Z. Fadil, A. Mhirech, B. Kabouchi, L. Bahmad and **W. Ousi Benomar**

Laboratoire de Matière Condensée et Sciences Interdisciplinaires (LaMCScI), Faculty of Sciences, P.O. Box 1014, Mohammed V University in Rabat, Morocco.

Doi: https://doi.org/10.47011/16.4.6

Received on: 13/11/2021; Accepted on: 20/02/2022

Abstract: This paper concerns the investigation of the critical (H_C) and the saturation (H_S) magnetic fields behavior of the studied system as a function of different physical parameters. The Monte Carlo method is used to study the magnetic properties of the ferrimagnetic behavior of a double fullerene X_{60} core/shell-like nanostructure. Based on the Ising model, we focus our study on a system formed by a double sphere core/shell. The two spheres contain the spins $\sigma = \pm 1/2$ in the core surrounded by the spin $S = \pm 1, 0$ in the shell. Various types of magnetization curves have been established, depending on the competition among the exchange couplings, the crystal fields, and the temperature. The study reveals that the saturation magnetic field (Hs) is significantly influenced by variations in all exchange coupling parameters, whereas the critical magnetic field (Hc) is only mildly affected by these parameter variations. Moreover, the crystal field and temperature both influence the critical and saturation magnetic fields.

Keywords: Double fullerene core/shell-like structure, Magnetization plateaus, Monte Carlo simulations, Critical and saturation fields, External magnetic field.

1. Introduction

The fullerene structure is a carbon molecule that can have various shapes, including a hollow sphere, a line, etc. Among these forms, we find the spherical fullerenes named “buckminster fullerenes” or “buckyballs.” Cylindrical fullerenes are also referred to as carbon nanotubes (“buckytubes”) [1-6]. Fullerenes are comparable in structure to graphite, which is made of arranged graphene sheets of connected hexagonal rings [7-10]. Twelve pentagons are essential to shut the cage and C_{60} is the only structure that meets these experimental rules. Consequently, C_{70} exhibits remarkable structural solidness and stability. Its structure is shaped by two parts of C_{60} connected by a ring of carbon particles, giving it a rugby ball-like shape. Furthermore, there exists an infinite number of possible variations, ranging from the most common to the most exotic, which makes the fullerene family exceptionally diverse and rich in various structural arrangements. [11-19]. The fullerenes have been discovered for the first time in 1985. Their discovery has led to an entirely new understanding of the behavior of sheet materials, and it has opened an entirely new chapter of nanoscience and nanotechnology [20-22]. Fullerenes have been extensively studied for their wide range of properties, which positions them as potential candidates for various applications in the future. These properties include their potential as light-activated antimicrobial agents [23], their remarkable temperature resistance [24], their role in superconductivity [25], and their

Corresponding Author: Z. Fadil **Email**: fadilzakaria604@gmail.com

biocompatibility [26]. Nanomaterials based on fullerene have been utilized in gadgets designed for photovoltaic cells and biomedical devices [27]. The ability of these nanosystems to both donate and accept electrons suggests promising applications in the fields of batteries and advanced electronic devices [28-35]. The Ising model is one of the basic and essential models of statistical physics and material science. This model has been effectively amplified to depict different attractive nano frameworks and plays a noteworthy part in understanding attractive magnetic properties [36-38]. There are structures that can be described by multiple models, such as the Ising model, which is often considered a logical and reasonable choice [39-42]. In this research, the Monte Carlo simulation is applied to simulate the magnetization plateaus of the fullerene-type core/shell structure. Additionally, several applications, including computer simulations, have been developed in this field of research. Theoretical investigations have concentrated on these nanostructures to display their magnetic, dielectric, and thermodynamic properties via different methods of simulations [43-52]. In previous work, we have employed Monte Carlo simulation to examine the ground phase diagrams, as well as the magnetic and thermodynamic properties of the fullerene structure under the influence of several physical parameters [53].

In this paper, we investigate magnetization plateaus in a double fullerene core/shell system. The study employs Monte Carlo simulations with the Metropolis algorithm to explore how these plateaus vary with different significant physical parameters. The outline of this article is as follows: the model and method used are illustrated in Sec. 2; the Monte Carlo simulation details are presented in Sec. 3; finally, we complete the study with a conclusion in Sec. 4.

2. Model and Simulations Technique

Using Monte Carlo simulations, we study a ferrimagnetic double fullerene X_{60} / Y_{60} core/shell nanostructure, composed of a spin $\sigma = \pm 1/2$ in the core which is surrounded by the spin $S = \pm 1,0$ in the shell. X corresponds to atoms with spin σ (red balls) and Y represents the atoms with spin S (blue balls) See Fig. 1.

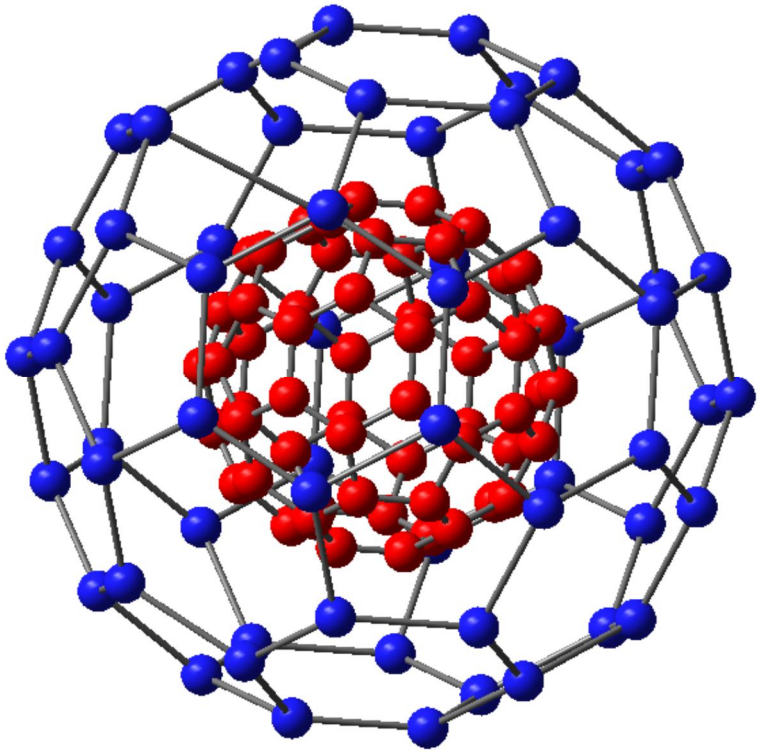

FIG. 1. Geometry of the double fullerene core/shell like-nanostructure.

In this figure, every spin is linked to the adjacent neighbor spins with different exchange coupling interactions. Furthermore, the interaction between two identical neighboring atoms (S-S) or (σ-σ) is considered to be ferromagnetic, while the interaction between the two atoms S and σ is considered to be ferrimagnetic.

The Ising Hamiltonian of the studied system, with different kinds of spins, including the exchange coupling interactions, the external magnetic field H, and the crystal field D, is given as follows:

$$\mathcal{H} = -J_C \sum_{\langle i,j \rangle} \sigma_i \sigma_j - J_S \sum_{\langle k,l \rangle} S_k S_l - J_{CS} \sum_{\langle m,n \rangle} \sigma_m S_n - H\left(\sum_i \sigma_i + \sum_j S_j\right) - D \sum_j S_j^2 \quad (1)$$

where <i, j>, < k, l>, and <m, n> stand for the first near neighbor spins (i and j), (k and l) and (m and n), respectively. Moreover, J_C, J_S, and J_{CS} are the exchange coupling constants between two first nearest neighbor atoms with spins σ-σ (in core), S-S (in shell), and S-σ (between core and shell), respectively. Each atom in the core and the shell interacts with the four nearest neighbors, three atoms surrounding it in its sphere and one atom in the opposite sphere.

To stimulate the Hamiltonian of Eq. (1), we apply the standard Monte Carlo technique under the Metropolis algorithm. The studied system involves the overall number of spins $N = N_S + N_\sigma = 120$. In this context, N_σ represents the number of spins in the shell, while N_S represents the number of spins in the core. Both N_σ and N_S are equal to 60.

To guarantee consistency, we produce the data with 10^6 Monte Carlo steps (MCS) per site after discarding the first 10^5 steps to reach the equilibrium, generating new configurations according to the Boltzmann distribution, in the reason to balance the present system and average over different initial conditions. Hereafter, we define the studied physical parameters as follows:

The magnetizations per spin are:

$$M_S = \frac{1}{N_S} \sum_i S_i \quad (2)$$

$$M_\sigma = \frac{1}{N_\sigma} \sum_j \sigma_j \quad (3)$$

The total magnetization is given by:

$$m_{tot} = \frac{M_S + M_\sigma}{2} \quad (4)$$

The internal energy per site is:

$$E = \frac{1}{N} \langle \mathcal{H} \rangle \quad (5)$$

3. Results and Discussion

In this section, we shall present some typical magnetic properties of the ferrimagnetic fullerene core/shell like-nanostructure. We focus on the effects of different physical parameters on the magnetization plateaus of this nanostructure, and we explore the behavior of the critical (H_C) and saturation (H_S) external magnetic fields by varying the exchange coupling interactions, the temperature, and the crystal field. The typical results are presented in Ref. [54].

In Fig. 2(a), we present the variation of the total magnetization as a function of the external magnetic field, for fixed exchange coupling coefficient values: $J_S = 0.1$ and $J_C = 1$, in the absence of the crystal field acting on S-spins. Thus, the following results for the magnetization plateaus were examined for T = 0.3 and various exchange coupling parameter values J_{CS} = -0.1, -0.2, -0.3, and -0.5.

From this figure, all magnetizations start from the value M_{tot} = -0.75 and saturate for the value M_{tot} = 0.75. Furthermore, two magnetization plateaus are localized at M_{tot} = 0.25 and 0.75, corresponding to the spin configurations (-1/2, +1) and (+1/2, +1), respectively. The first plateau appears for the critical magnetic fields (H_C) while the second is reached for the saturation magnetic field (H_S). Furthermore, it is found that the critical magnetic field value Hc decreases when increasing the J_{CS} parameter in its absolute values, whereas the saturation magnetic field value Hs increases when increasing the J_{CS} parameter in its absolute values [55].

To clarify the behavior of the Hs and Hc, we collect the obtained values in Fig. 2(a) to plot, in Fig. 2(b), the external magnetic fields as a function of the exchange coefficient coupling in its absolute value ($|J_{CS}|$). Indeed, when increasing the parameter J_{cs} in its absolute values, the magnetic field (Hs) increases while the critical magnetic field (Hc) decreases linearly. Such behavior is due to the ferrimagnetic coefficient coupling that tends to align the spins anti-parallel to each layer existing in the core and the shell of the double fullerene.

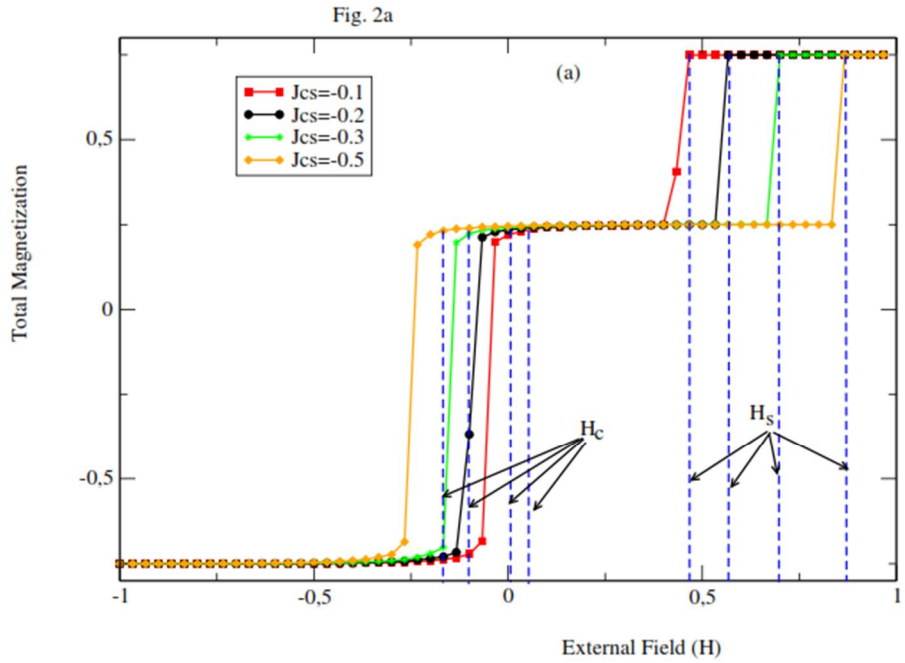

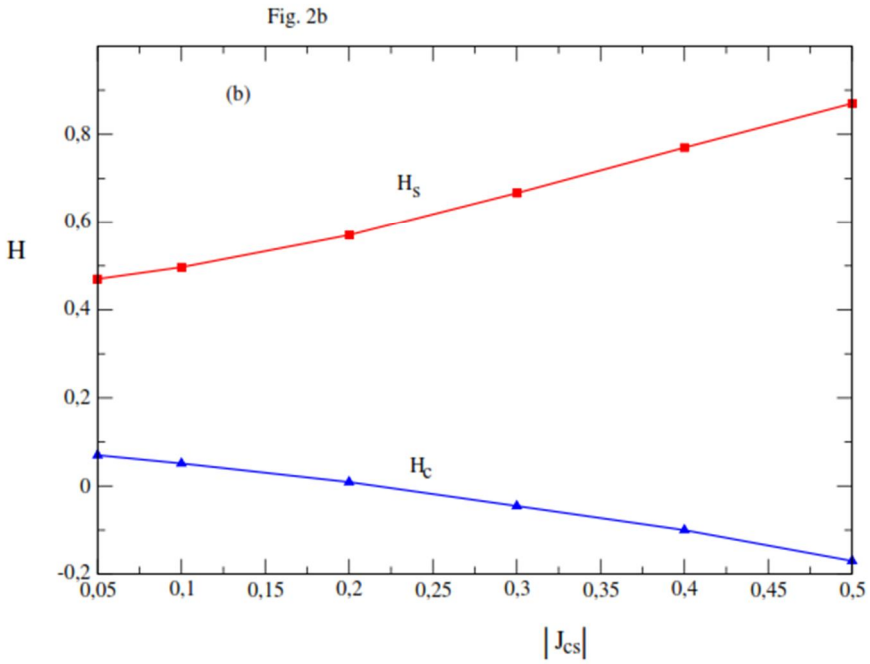

FIG. 2. The total magnetization as a function of the external magnetic field (a) and the external magnetic field versus $|J_{CS}|$ (b), for $J_C = 1$, $J_S = 0.1$, D = 0, and T = 0.3.

Figure 3(a) shows the total magnetization as a function of the external magnetic field for different values of the J_S parameter. This figure is plotted for fixed exchange coupling coefficient values: $J_{CS} = -0.1$, $J_C = 1$, in the absence of the crystal field (D = 0), and for the temperature T = 0.3. We can see that all total magnetization curves start from the same value (-0.75) corresponding to the configuration (-1/2, -1) and it remains constant, then the magnetizations undergo a second-order transition for $J_S < 0.1$ and a first-order transition for $J_S \geq 0.1$. Besides, this figure represents four magnetization plateaus (-0.25, -0.75, 0.25, and 0.75), and the distinct values of magnetic fields are highlighted by dash lines and illustrate the (Hs) where the total magnetization approaches the saturation value 0.75. Moreover, H_c is presented by the dash lines, where the total magnetization plateaus are equal to -0.25 and 0.25. Furthermore, the important result obtained in Fig. 3(a) resides in the fact that the intermediate plateau corresponding to $M_{tot} = 0.25$ obtained for Js < 0.4 is replaced by the plateau relating to $M_{tot} = -0.25$ for Js ≥ 0.4.

Collecting the data in Fig. 3(a), we illustrate, in Fig. 3(b), the behavior of the exchange coupling in the shell J_S when varying the external magnetic field. We can see clearly that the critical magnetic field, Hc, starts from the value 0.3, decreases, and subsequently increases for Js < 0.3. It then continues to increase and stabilizes for Js ≥ 0.3. We notice that Hc gets remarkably influenced by the spins in the shell. Conversely, Hs, the saturation field, varies slightly for Js < 0.3 and then increases almost linearly when Js ≥ 0.3. Therefore, the effect of the exchange coupling Js on the critical Hc and saturation Hs fields is significant.

Fig. 3a

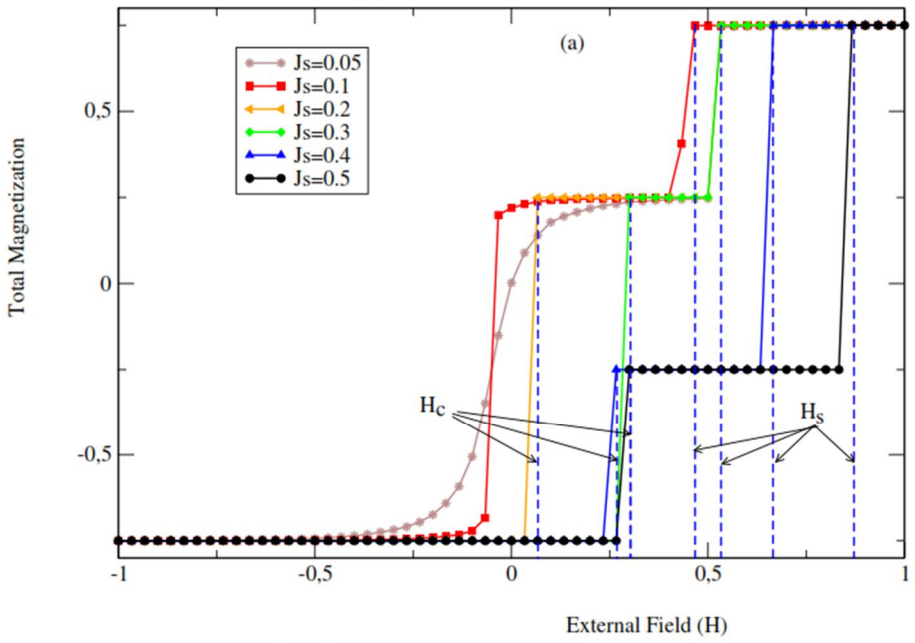

Fig. 3b

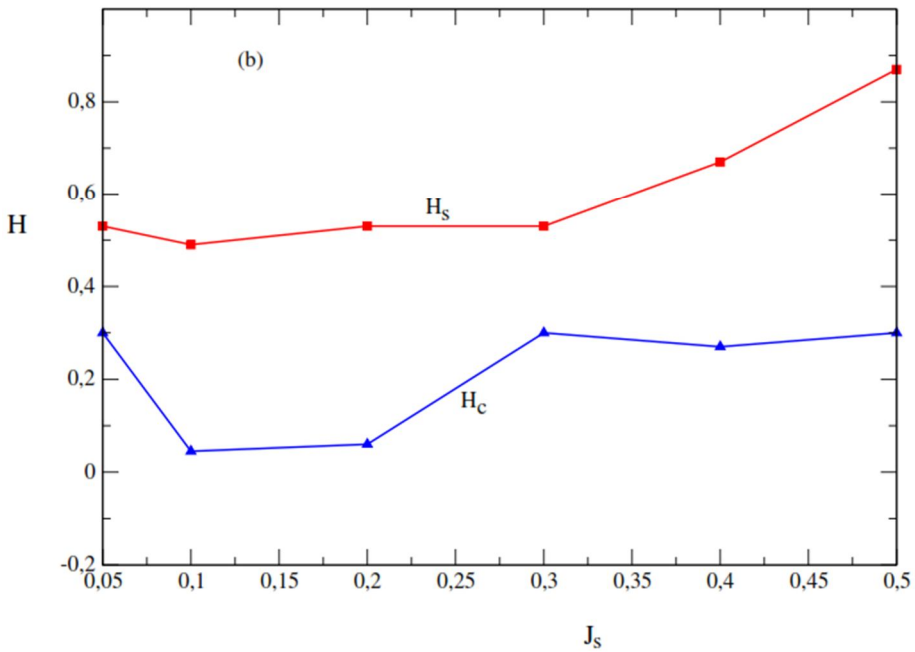

FIG. 3. The total magnetization as a function of the external magnetic field (a) and the external magnetic field versus J_S (b), for $J_C = 1$, $J_{CS} = -0.1$, D = 0, and T = 0.3.

Following the same motivation, the Figs. 4(a) and 4(b), present the effect of the exchange coupling in the core J_C (J_C = 0.1, 1, 2, 3, 4, and 5) on the critical Hc and saturation Hs fields for fixed parameters: $J_S = 0.1$, $J_{CS} = -0.1$, D = 0, and T = 0.3. There is a first magnetization plateau M = +0.25 related to the configuration (-1/2, +1), corresponding to a zero critical external

magnetic field value (Hc = 0) regardless of the values of J_C. Besides, when increasing the external magnetic field, a second plateau is reached. However, the passage between the two plateaus takes place by a first-order transition located at the saturation magnetic field (Hs). Such saturation magnetic field increases when increasing the parameter J_C. Indeed, the saturation magnetic field values are Hs = 0.75, 2.2, 5.1, 7.5, and 9.2 corresponding to the value of J_C = 1, 2 3, 4, and 5, respectively. To better illustrate this behavior, we plot Fig. 4(b) with the same values of the fixed physical parameters taken in Fig. 4(a). It is clear that Hc remains constant even when we increase the coefficient J_C, while the saturation magnetic field Hs increases strongly and linearly with the increase of J_C. Therefore, J_C has no effect on the critical magnetic field Hc and the behavior of the Hs comes from the dominant effect of the external magnetic field.

Fig. 4a

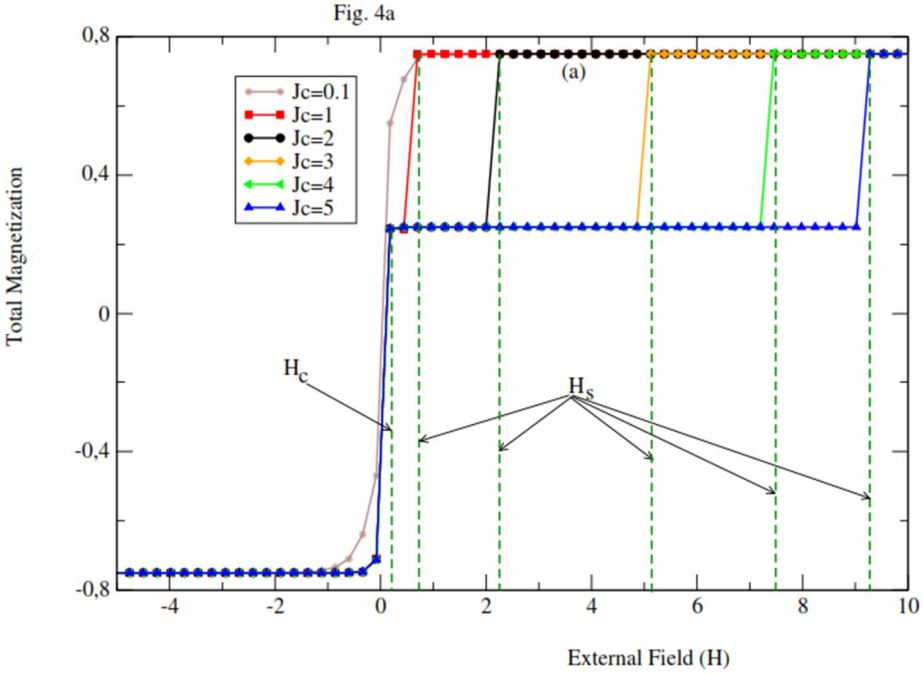

Fig. 4b

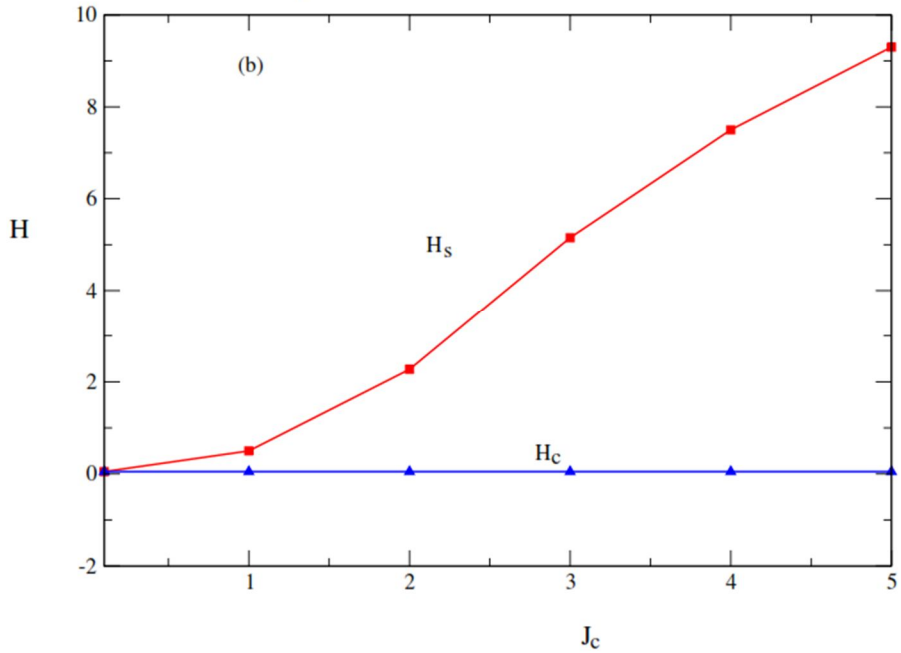

FIG. 4. Total magnetization as a function of the external magnetic field (a), the external magnetic field versus J_C (b), for J_S = 0.1, J_{CS} = -0.1, D = 0, and T = 0.3.

To focus on the effect of the temperature, we present in Figs. 5(a) and 5(b) the variation of the total magnetization versus external magnetic field for different temperature values (T = 0.05, 0.1, 0.2, 0.3, 0.4, and 0.5). These figures are plotted in the absence of the crystal field and for fixed values of J_C = 1, J_S = 0.1, and J_{CS} = -0.1. The appearance of intermediate magnetization plateaus is found only for the configuration (-1/2, +1) corresponding to M_{tot} = 0.25. All values of the critical magnetic field appear for temperatures below 0.5. Indeed, for temperatures below 0.5, the critical magnetic field (Hc) varies slightly. Whereas, for temperatures greater than or equal to 0.5, the intermediate plateau disappears. On the other hand, the plateau corresponding to saturation of the total magnetization increases when the temperature is increased, inducing a decrease in H_S.

Collecting the results obtained in Fig. 5(a), we plot Fig. 5(b). This figure shows the variation of Hc and Hs as a function of the temperature. Contrasting to Fig. 4(b), in this figure, Hs decreases with the temperature from Hc = 2.4 until reaching the value of Hc = 0.4. The results obtained from these two figures can be explained by the competition between the temperature and H since the external magnetic field tends to make the spins in a parallel direction while the temperature effect is to disorder the studied system.

Fig. 5a

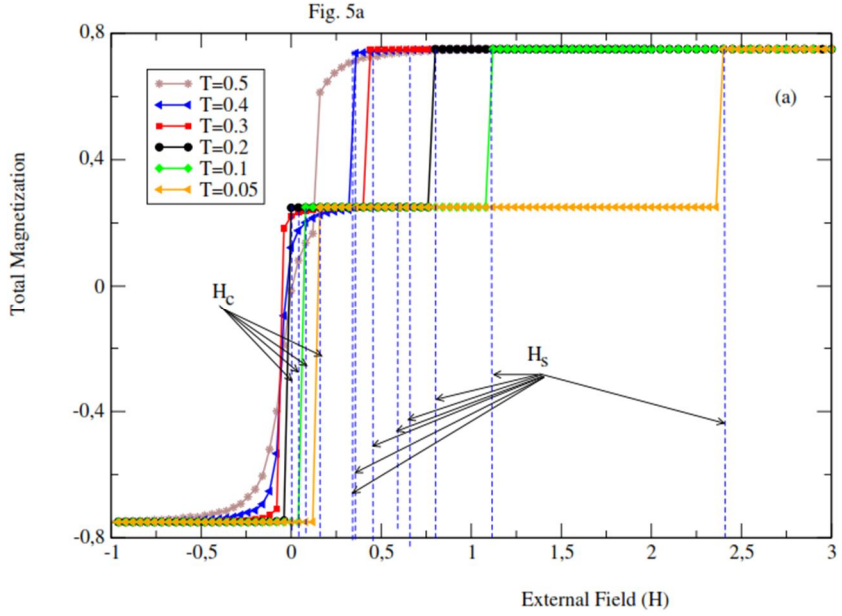

Fig. 5b

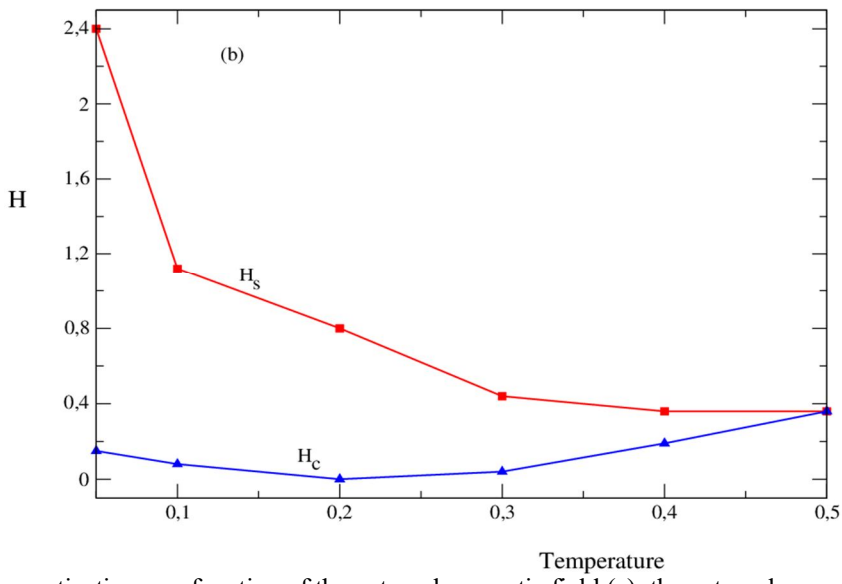

FIG. 5. Total magnetization as a function of the external magnetic field (a), the external magnetic field versus temperature (b), for J_C = 1, J_C = 0.1, J_{CS} = -0.1, and D = 0.

Finally, to complete this study, we exhibit Figs. 6(a) and 6(b) to investigate the influence of the crystal field D on the magnetization plateaus. These figures are plotted for fixed parameter values: $J_C = 1$, $J_S = 0.1$, $J_{CS} = -0.1$, and $T = 0.3$. By varying the external magnetic field, for several values of crystal field, the total magnetization varies from -0.75 to 0.75, passing through two plateaus. The first plateau corresponds to $M_{tot} = -0.25$ and the second one to $M_{tot} = 0.25$. The transition from one plateau to another is made by first-order transitions [56]. The first and second plateaus are reached for the critical values H_{C1} and H_{C2} of the external magnetic field, respectively, while the last saturation plateau is reached for the value Hs. The important result revealed by Fig. 6(a) resides in the fact that the effect of the crystal field variation is felt only for its negative values. On the other hand, for the positive values of the crystal field, the two intermediate plateaus disappear.

Fig. 6a

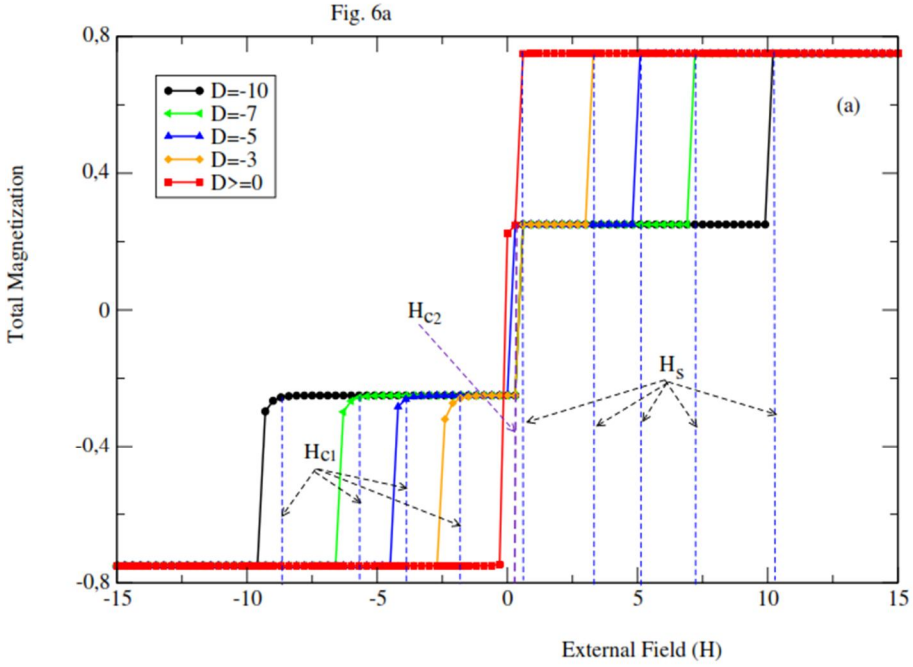

Fig. 6b

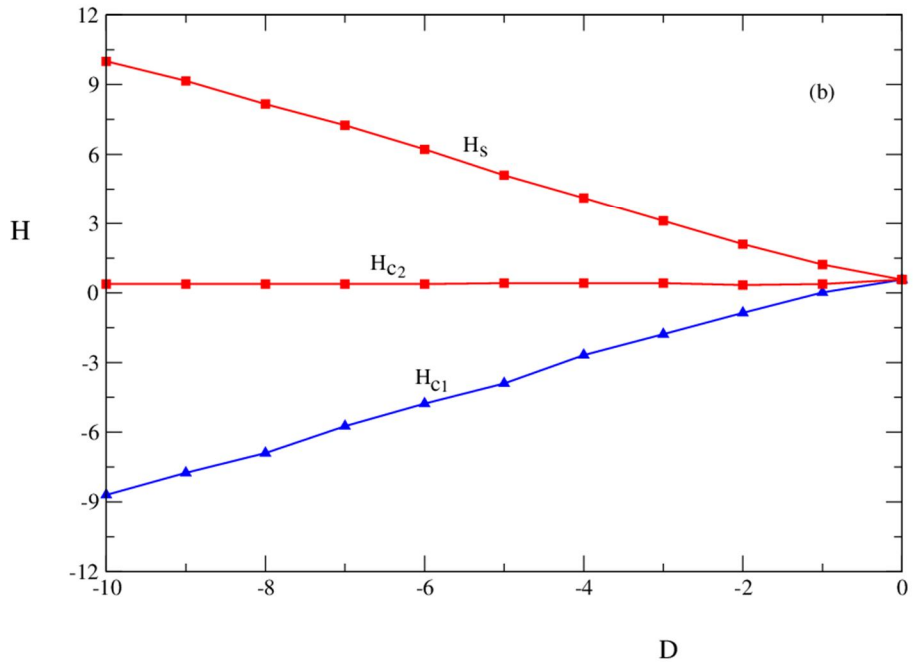

FIG. 6. Total magnetization as a function of the external magnetic field (a), the external magnetic field versus the crystal field (b), for $J_C = 1$, $J_S = 0.1$, $J_{CS} = -0.1$, and $T = 0.3$.

The values of H_{C1} increase within the range of approximately -11 to 1.8. Simultaneously, the values of H_S decrease from 10.4 to 0.5, while H_{C2} remains almost constant. These results are collected and plotted in Fig. 6(b). As you can see, as the parameter D increases, H_{c1} shows a linear increase until D reaches 0. Meanwhile, H_{c2} is not affected and maintains a constant value. Conversely, H_S decreases linearly as D increases. H_S, H_{c1}, and H_{c2} converge at the point where D equals 0. The symmetry of the plates concerning the axis H = 0 is reflected by the curves H_S and H_{c1}. Such results can be explained by the competition between the three physical parameters, including D, H, and J_{CS}. The external magnetic field H tends to force the spins of each layer in the core and in the shell to align along their direction, whereas the ferrimagnetic exchange coupling J_{CS} tends to maintain them in antiparallel alignment. On the other hand, we remark that, when decreasing the crystal field, the critical magnetic field H_{c1} decreases and the saturation magnetic field Hs increases. While the critical magnetic field H_{c2} is not affected by the variation of the crystal field, it can be explained by the increase of the external magnetic field.

4. Conclusion

Using the Monte Carlo simulations, we have investigated the magnetization plateaus' behaviors of a double fullerene core/shell structure under the influences of specific physical parameters: the exchange couplings, temperature, and the crystal field in an external magnetic field. Additionally, the magnetization plateaus, the critical (H_C), and the saturation (H_S) magnetic fields have been investigated. It is found that the exchange coupling in the core affects strongly the saturation magnetic field, whereas the exchange coupling in the shell influences the critical magnetic field. Moreover, the crystal field has a remarkable impact on both the critical and saturation fields. Indeed, the negative values of D allow having two intermediate plateaus. These plateaus disappear when D is positive.

References

[1] Abhijit, R., Asian J. Pharm. Res., 2 (2012) 47.

[2] Enyashin, A. N. and Ivanovskii, A. L., Chem. Phys. Lett., 473 (2009) 108.

[3] Iyakutti, K., Rajarajeswari, M. and Kawazoe, Y., Physica B, 405 (2010) 3324.

[4] Zhao, C-X., Yang, Y-Q., Niu, C-Y., Wang, J-Q. and Jia, Y., Comput. Mater. Sci., 160 (2019) 115.

[5] Lv, Y., Wang, H., Guo, Y., Jiang, B. and Cai, Y., Comput. Mater. Sci., 144 (2018) 170.

[6] Zhu, X., Yan, H., Wang, X., Zhang, M. and Wei, Q., Results Phys., 15 (2019) 102738.

[7] Terrones, M. *et al*., Nano Today, 5 (2010) 351.

[8] Lusk, M.T. and Carr, L.D., Carbon, 47 (2009) 2226.

[9] Lekakh, S.N., Zhang, X., Tucker, W., Lee, H.K., Selly, T. and Schiffbauer, J.D., Mater. Charact., 158 (2019) 109991.

[10] Ma, R., Zhou, Y., Bi, H., Yang, M., Wang, J., Liu, Q. and Huang, F., Prog. Mater. Sci., (2020) 100665. (in proof)

[11] Adhikari, S. and Chowdhury, R., Phys. Lett. A, 375 (2011) 2166.

[12] Satoh, M. and Takayanagi, I., J. Pharmacol. Sci., 100 (2006) 513.

[13] Pan, Y., Liu, X., Zhang, W., Liu, Z., Zeng, G., Shao, B., Liang, Q., He, Q., Yuan, X., Huang, D. and Chen, M., Appl. Catal. B-Environ., 265 (2020) 118579.

[14] Konno, T., Wakahara, T., Miyazawa, K. and Marumoto, K., New Carbon Mater., 33 (2018) 310.

[15] Ahmad, S., Chem. Phys. Lett., 713 (2018) 52.

[16] Tapia, J.I., Larios, E., Bittencourt, C., Yacamán, M.J. and Quintana, M., Carbon, 99 (2016) 541.

[17] Bondavalli, P., "Graphene and Related Nanomaterials: Properties and Applications", (Elsevier, 2018).

[18] Sachdeva, S., Singh, D. and Tripathi, S.K., Opt. Mater., 101 (2020) 109717.

[19] Borisova, P.A., Blanter, M.S., Brazhkin, V.V., Lyapin, S.G., Somenkov, V.A., Filonenko, V.P., Trenikhin, M.V. and Presniakov, M.Yu., Diam. Relat. Mater., 85 (2018) 74.

[20] Smalley, R.E., Rev. Mod. Phys., 69 (1997) 723.

[21] Avent, A.G., Benito, A.M., Birkett, P.R., Darwish, A.D., Hitchcock, P.B., Kroto, H.W., Locke, I.W., Meidine, M.F., O'Donovan, B.F., Prassides, K., Taylor, R., Walton, D.R.M. and van Wijnkoop, M., J. Mol. Struct., 436–437 (1997) 1.

[22] Tang, Y., Li, J., Du, P., Zhang, H., Zheng, C., Lin, H., Du, X. and Tao, S., Org. Electron., 83 (2020) 105747.

[23] Heredia, A-D., Durantini, A-M., Durantini, J-E. and Durantini, E-N., J. Photoch. Photobio. C, 51 (2022) 100471.

[24] Wu, B-S., An, M-W., Chen, J-M., Xing, Z., Chen, Z-C., Deng, L-L., Tian, H-R., Yun, D-Q., Xie, S-Y. and Zheng, L-S., Cell Rep. Phys. Sci., 2 (2021) 100646.

[25] Kantar, E., Solid State Commun., 263 (2017) 31.

[26] Sharoyko, V-V., Shemchuk, O-S., Meshcheriakov, A-A., Vasina, L-V., Iamalova, N-R., Luttsev, M-D., Ivanova, D-A., Petrov, A-V., Maystrenko, D-N., Molchanov, O-E. and Semenov, K-N., Nanomed.-Nanotechnol., 40 (2022) 102500.

[27] Sun, H., Chen, F. and Chen, Z-K., Mater. Today, 24 (2019) 94.

[28] Kuznietsova, H-M., Dziubenko, N-V., Lynchak, O-V., Herheliuk, T-S., Zavalny, D-K., Remeniak, O-V., Prylutskyy, Y-I. and Ritter, U., Digest. Dis. Sci., 65 (2020) 215.

[29] Yan, Y., Zhang, K., Wang, H., Liu, W., Zhang, Z., Liu, J. and Shi, J., Colloid Surface B, 186 (2020) 110700.

[30] Bernal Texca, F.G., Chigo-Anota, E., Tepech Carrillo, L. and Castro, M., Comput. Theor. Chem., 1103 (2017) 1.

[31] Zhang, Y., Zhang, C-R., Yuan, L-H., Zhang, M-L., Chen, Y-H., Liu, Z-J. and Chen, H-S., Mater. Chem. Phys., 204 (2018) 95.

[32] Benatto, L., Marchiori, C-F-N., Talka, T., Aramini, M., Yamamoto, N-A-D., Huotari, S., Roman, L-S. and Koehler, M., Thin Solid Films, 697 (2020) 137827.

[33] Meng, Q-Y., Zhang, B. and Wang, D-L., Comput. Theor. Chem., 1173 (2020) 112672.

[34] Goodarzi, S., Ros, T-D., Conde, J., Sefat, F. and Mozafari, M., Mater. Today, 20 (2017) 460.

[35] Lu, X., Cui, M., Pan, X., Wang, P. and Sun, L., Appl. Surf. Sci., 503 (2020) 144328.

[36] Moodie, J.C., Kainth, M., Robson, M.R. and Long, M.W., Physica A, 541 (2020) 123276.

[37] Ertaş, M. and Keskin, M., Physica A, 526 (2019) 120933.

[38] Freitas, A.S., Douglas, F., Fittipaldi, I.P. and Moreno, N.O., J. Magn. Magn. Mater., 362 (2014) 226.

[39] Berkai, Z., Daoudi, M., Mendil, N. and Belghachi, A., Phys. Lett. A, 383 (2019) 2090.

[40] Maaouni, N., Qajjour, M., Mhirech, A., Kabouchi, B., Bahmad L. and Ousi Benomar, W., J. Magn. Magn. Mater., 468 (2018) 175.

[41] Qajjour, M., Maaouni, N., Fadil, Z., Mhirech, A., Kabouchi, B., Ousi Benomar, W. and Bahmad, L., Chinese J. Phys., 63 (2020) 36.

[42] Fadil, Z., Qajjour, M., Mhirech, A., Kabouchi, B., Bahmad, L. and Ousi Benomar, W., Physica B, 564 (2019) 104.

[43] Benhouria, Y., Essaoudi, I., Ainane, A. and Ahuja, R., Physica E, 108 (2019) 191.

[44] Wang, J.M., Jiang, W., Zhou, C.L., Shi, Z. and Wu, C., Superlattice Microst., 102 (2017) 359.

[45] Fadil, Z., Maaouni, N., Mhirech, A., Kabouchi, B., Bahmad, L. and Ousi Benomar, W., Braz. J. Phys., 50 (2020) 716.

[46] Fadil, Z., Mhirech, A., Kabouchi, B., Bahmad, L. and Ousi Benomar, W., Phys. Lett. A, 384 (2020) 126783.

[47] Moujaes, E-A., Aguiar, L-V. and Abou Ghantous, M., J. Magn. Magn. Mater., 423 (2017) 359.

[48] Fadil, Z., Mhirech, A., Kabouchi, B., Bahmad, L. and Ousi Benomar, W., Chinese J. Phys., 67 (2020) 123.

[49] Jander, P., Santos, F.C. and Barreto, S., J. Magn. Magn. Mater., 439 (2017) 114.

[50] Wu, C., Shi, K.L., Zhang, Y. and Jiang, W., J. Magn. Magn. Mater., 465 (2018) 114.

[51] Fadil, Z., Qajjour, M., Mhirech, A., Kabouchi, B., Bahmad, L. and Ousi Benomar, W., Ferroelectrics, 573 (2021) 141.

[52] Fadil, Z., Mhirech, A., Kabouchi, B., Bahmad, L. and Ousi Benomar, W., Chinese J. Phys., 64 (2020) 295.

[53] Aouini, S., Mhirech, A., Alaoui-Ismaili, A. and Bahmad, L., Chinese J. Phys., 59 (2019) 346.

[54] Fadil, Z., Mhirech, A., Kabouchi, B., Bahmad, L. and Ousi Benomar, W., Integr. Ferroelectr., 213 (2021) 146.

[55] Wang, Z., Li, Q., Wang, F., Sun, L., Tian, M. and Wang, W., Superlattice Microst., 136 (2019) 106293.

[56] Bonetti, E., Fabrice, M. and Fremond, M., J. Math. Anal. Appl., 384 (2011) 561.